Progress In Electromagnetics Research, Vol. 139, 57–86, 2013

PERFORMANCE EVALUATION OF DFT BEAMFORMERS FOR BROADBAND ANTENNA ARRAY PROCESSING

Yen-Lin Chen[1] and Ju-Hong Lee[2, 3, *]

[1]Graduate Institute of Communication Engineering, National Taiwan University, No. 1, Sec. 4, Roosevelt Rd., Taipei 10617, Taiwan

[2]Department of Electrical Engineering, Graduate Institute of Communication Engineering, National Taiwan University, No. 1, Sec. 4, Roosevelt Rd., Taipei 10617, Taiwan

[3]Graduate Institute of Biomedical Electronics and Bioinformatics, National Taiwan University, No. 1, Sec. 4, Roosevelt Rd., Taipei 10617, Taiwan

Abstract—Broadband beamforming has been an important issue on antenna array processing due to many practical demands on communication, radar, or sonar applications. Although several effects deteriorating array performance have been addressed for narrowband beamforming, few of them are considered for the broadband scenario. Besides, the definition of output signal-to-interference plus noise ratio (SINR) and the way to simulate broadband signal sources are usually vague, which further obstructs the development of broadband beamforming. In this paper, the performance of discrete Fourier transform (DFT) beamformers operating in block processing and sliding window modes are investigated when the correlation matrices are known or estimated by finite data samples. The output SINR of DFT beamformers is well-defined, and the generation of broadband signals is clearly introduced. Simulation results with respect to the signal bandwidth, the number of frequency bins, and the number of data samples are presented for illustration and comparison.

1. INTRODUCTION

Adaptive beamforming has been developed in past decades due to its significant anti-jamming ability. Ideally, an adaptive array can

Received 16 February 2013, Accepted 15 April 2013, Scheduled 17 April 2013

* Corresponding author: Ju-Hong Lee (juhong@cc.ee.ntu.edu.tw).

eliminate the interference and noise efficiently while protecting the desired signal source arriving from a specific direction. However, the performance of adaptive antenna arrays can be deteriorated by several errors in practical situation such as steering vector errors [1], finite sample effect [2], source coherence [3], mutual coupling [4], etc.. Many robust techniques were proposed to cope with these effects on array performance. Notables among them are eigenspace-based method [5], diagonal loading technique [6], signal blocking [7], and spatial smoothing [8]. Although the unwanted effects are circumvented by a variety of methods, most of the adaptive beamforming techniques are limited to the scope of narrowband signal environment and narrowband beamforming. In practice, many applications such as sonar [9], radar [10], communication [11], and microphone array [12] are not strictly narrowband. Since signal sources with nonzero bandwidth degrade the performance of an adaptive array [13, 14], a broadband beamformer is necessary in broadband environments to alleviate the effect of signal bandwidth.

Usually, adaptive beamformers for broadband signal reception are classified to two structures: the tapped delay-line (TDL) beamformer and the discrete Fourier transform (DFT) beamformer [15] (also note the recently proposed structure called sensor delay-line in [16, 17]). In the TDL beamformer, the time-domain data vectors $\{\mathbf{x}[n]\}_{n=0\sim N-1}$ are directly weighted by a set of coefficients satisfying certain constraint and optimization problem [18]. Due to its effectiveness, the TDL beamformer has been the most popular scheme and is widely considered for broadband beamforming [13, 19, 20]. Several publications discussing the TDL beamformer suffering from look direction errors have been reported recently [21, 22]. On the other hand, the DFT beamformer transforms the time-domain data vectors $\{\mathbf{x}[n]\}_{n=0\sim N-1}$ to frequency-domain via DFT, processes each frequency bin by a narrowband beamformer, and then performs the inverse DFT (IDFT) to obtain the time-domain outputs. The DFT beamformer is computational efficient since the matrices to be inverted in computing weights have lower dimension. This property has been utilized to calculate the weight coefficients of the TDL beamformer by the frequency-domain method [22–25]. Several applications of the DFT beamformer in communication systems are available in [26–28].

The connection between the TDL and DFT beamformers has been studied in [23, 29]. The investigation in [29] reveals that the output signal-to-interference-plus-noise ratio (SINR) of the DFT beamformer is identical to that of the TDL beamformer. In other words, the DFT operation cannot provide any improvement on array performance. However, the analysis of [29] only considers the case where the *entire*

weight vector is computed by the LMS or Applebaum algorithms. Since the weight vector in each frequency bin of the DFT beamformer is usually produced individually, the conclusion of [29] may not be appropriate for all kinds of DFT beamformers. In spite of the existing work in [22–30], the output SINR of the DFT beamformer is never well-defined and studied in detail. Moreover, the performance of the DFT beamformer with correlation matrices estimated by finite data samples are seldom evaluated or discussed in the literature. Therefore, we investigate the performance and capabilities of the DFT beamformer in broadband array processing in this paper. The main contributions are listed as follows:

1. The definition of the output SINR for DFT beamformers in terms of weight vectors is established explicitly and clearly. This provides a fair comparison to different algorithms and prevents the ambiguity for the broadband performance metric. The narrowband beamforming and narrowband sources scenario are the special cases of our results, which validates this work.
2. In addition to the perfect case that the correlation matrices of the data vectors are known to the receiver, the finite sample effect on DFT beamformers is also considered and observed by simulation results. Different from most of the existing literature, the method used to generate the sample points of broadband white Gaussian sources for simulation is described in detail. This facilitates the field of exploring the finite sample effect in broadband beamforming.
3. The DFT beamformers operating in block processing mode and sliding window mode are both included. The output SINRs of them under the perfect (the correlation matrices are known) and imperfect (the correlation matrices are estimated by finite samples) situations are examined and compared with those of the narrowband minimum variance distortionless response (MVDR) and broadband TDL beamformers. This investigation confirms the effectiveness of the DFT beamformers in alleviating the sensitivity of an antenna array system to signal bandwidth. Besides, the presented results indicate that the performance of the TDL beamformer can be severely deteriorated by the finite sample effect.

The paper is organized as follows. The expression of the broadband received signal and the schemes of DFT beamformers in block processing and sliding window modes are introduced in Section 2. The definitions of the output SINR for DFT beamformers with arbitrary signal bandwidth are derived in Section 3. The output

SINRs of several classical narrowband and broadband beamformers are compared by the simulation results in Section 4. Finally, we make a conclusion in Section 5.

2. PRINCIPLES OF BROADBAND BEAMFORMERS

2.1. Received Signal Model

Consider D stationary, uncorrelated, zero-mean sources including one desired signal and D-1 interferers are impinging on an M-element array with arbitrary geometry. The diagram of an adaptive array system is illustrated in Figure 1. First, the received signal of each sensor passes through an ideal bandpass filter with center frequency f_c and bandwidth $2B$. The band-limited received signal of the mth element and its Hilbert transform are respectively given by

$$x_{m,I}(t) = s_{1,I}(t+\tau_{1,m}) + \ldots + s_{D,I}(t+\tau_{D,m}) + w_{m,I}(t) \quad (1)$$

and

$$x_{m,Q}(t) = s_{1,Q}(t+\tau_{1,m}) + \ldots + s_{D,Q}(t+\tau_{D,m}) + w_{m,Q}(t), \quad (2)$$

where $w_{m,I}(t)$ and $w_{m,Q}(t)$ are the band-limited spatially white noise with zero-mean and $\tau_{d,m}$ is the propagation delay of the dth source and mth element with respect to the reference point. The in-phase and quadrature-phase of the dth band-limited signal carrying amplitude $\alpha_d(t)$ and phase $\phi_d(t)$ are expressed as

$$s_{d,I}(t) = \alpha_d(t)\cos(2\pi f_c t + \phi_d(t)) \quad (3)$$

and

$$s_{d,Q}(t) = \alpha_d(t)\sin(2\pi f_c t + \phi_d(t)), \quad (4)$$

$d = 1, 2, \ldots, D$, respectively. Without loss of generality, we assume that the first signal source, i.e., $d = 1$, denotes the desired signal and

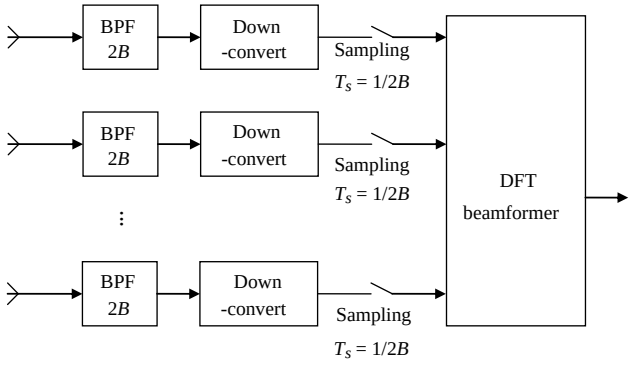

Figure 1. System diagram of an adaptive array.

the others interference. Using (1)–(4), the analytical signal is given by

$$\begin{aligned} x_{m,+}(t) &= x_{m,I}(t) + jx_{m,Q}(t) \\ &= \alpha_1(t+\tau_{1,m})\exp\{j[2\pi f_c(t+\tau_{1,m}) + \phi_1(t+\tau_{1,m})]\} \\ &\quad + \ldots + \alpha_D(t+\tau_{D,m})\exp\{j[2\pi f_c(t+\tau_{D,m}) \\ &\quad + \phi_D(t+\tau_{D,m})]\} + w_{m,+}(t) \end{aligned} \tag{5}$$

with corresponding noise $w_{m,+}(t)$, $m = 1, 2, \ldots, M$. After down-converting the RF signal to the baseband, the received signal of the mth element is given by

$$\begin{aligned} x_m(t) &= x_{m,+}(t)\exp(-j2\pi f_c t) = s_1(t+\tau_{1,m})\exp\{j2\pi f_c\tau_{1,m}\} \\ &\quad + \ldots + s_D(t+\tau_{D,m})\exp\{j2\pi f_c\tau_{D,m}\} + w_m(t), \end{aligned} \tag{6}$$

where $s_d(t) = \alpha_d(t)\exp\{j\phi_d(t)\}$ is the complex envelope of the dth signal source, and $w_m(t)$ is the complex envelope of the noise in the mth element. By sampling $x_m(t)$ at Nyquist rate $t = nT_s = n/2B$ with T_s denoting the sampling interval, the nth snapshot of the received signal is written as

$$\begin{aligned} x_m(nT_s) &= s_1(nT_s+\tau_{1,m})\exp\{j2\pi f_c\tau_{1,m}\} \\ &\quad + \ldots + s_D(nT_s+\tau_{D,m})\exp\{j2\pi f_c\tau_{D,m}\} + w_m(nT_s). \end{aligned} \tag{7}$$

Equation (6) is a general expression for the received signals with an arbitrary bandwidth. We assume that the autocorrelation functions of the random processes $s_d(t)$ and $w_m(t)$ are respectively $r_d(\xi)$ and $r_w(\xi)$ throughout this paper. Since $w_m(t)$, $m = 1, 2, \ldots, M$, are band-limited white noise, the samples $w_m(nT_s)$ with $T_s = 1/2B$ are uncorrelated with identical distribution. Note that $s_d(t)$ are band-limited but not necessarily white. If the bandwidth B is much less than the carrier frequency f_c, the baseband signal $s_d(t)$ are almost invariant during the time difference $\tau_{d,m}$ for all m. Therefore, the received narrowband signal can be approximately written as

$$x_m(t) \approx s_1(t)\exp\{j2\pi f_c\tau_{1,m}\} + \ldots + s_D(t)\exp\{j2\pi f_c\tau_{D,m}\} + w_m(t), \tag{8}$$

which is the signal model commonly used in narrowband beamforming. We can see that the time differences in (1) and (2) for distinct elements are simplified to phase differences in this case.

2.2. DFT Beamformers

There are two operation modes in DFT beamformers — block processing and sliding window. The scheme of the DFT beamformer with block processing is presented in Figure 2. Let $\mathbf{x}$ be the time-domain data matrix composed of N snapshots of the received signal

vector as follows:

$$\begin{aligned}\mathbf{x} &= [\mathbf{x}[0] \quad \mathbf{x}[1] \quad \mathbf{x}[2] \quad \ldots \quad \mathbf{x}[N-1]] \\ &= \begin{bmatrix} x_1[0] & x_1[1] & \ldots & x_1[N-1] \\ x_2[0] & x_2[1] & \ldots & x_2[N-1] \\ \vdots & \vdots & \ldots & \vdots \\ x_M[0] & x_M[1] & \ldots & x_M[N-1] \end{bmatrix} = \begin{bmatrix} \tilde{\mathbf{x}}_1^T \\ \tilde{\mathbf{x}}_2^T \\ \tilde{\mathbf{x}}_3^T \\ \vdots \\ \tilde{\mathbf{x}}_M^T \end{bmatrix}, \end{aligned} \tag{9}$$

where $(\cdot)^T$ denotes the matrix transpose, and $[n]$ is used to replace (nT_s) for simplicity. Performing DFT to the N data of each element, we have

$$\begin{aligned}\mathbf{X} &= [\mathbf{X}[0] \quad \mathbf{X}[1] \quad \mathbf{X}[2] \quad \ldots \quad \mathbf{X}[N-1]] \\ &= \begin{bmatrix} X_1[0] & X_1[1] & \ldots & X_1[N-1] \\ X_2[0] & X_2[1] & \ldots & X_2[N-1] \\ \vdots & \vdots & \ldots & \vdots \\ X_M[0] & X_M[1] & \ldots & X_M[N-1] \end{bmatrix}, \end{aligned} \tag{10}$$

where

$$X_m[k] = \sum_{n=0}^{N-1} x_m[n]\, e^{-j2\pi nk/N} = \mathbf{e}_k^H \tilde{\mathbf{x}}_m, \quad k = 0, 1, \ldots, N-1, \tag{11}$$

$$\mathbf{e}_k = [1 \quad \exp\{j2\pi k/N\} \quad \ldots \quad \exp\{j2\pi\,(N-1)\,k/N\}]^T, \tag{12}$$

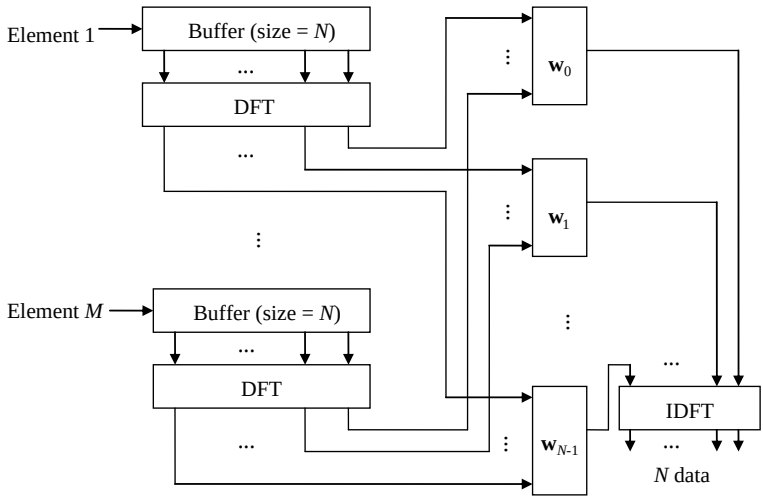

Figure 2. The scheme of the DFT beamformer in block processing mode.

and $(\cdot)^H$ represents the conjugate and transpose. In (10), $\mathbf{X}[k] = \mathbf{X}(f_k)$ denotes the $(k+1)$th frequency component of the received signal and

$$f_k = \begin{cases} k \cdot \Delta f, & k = 0 \sim \text{ceil}\,(N/2) - 1 \\ (k - N) \cdot \Delta f, & k = \text{ceil}\,(N/2) \sim (N-1) \end{cases} \tag{13}$$

with frequency resolution $\Delta f = 1/NT_s$. The symbol ceil$(\cdot)$ denotes rounding toward positive infinity. Once the frequency-domain data matrix of (10) is obtained, each frequency component (i.e., each column of $\mathbf{X}$) is processed by a narrowband beamformer $\mathbf{w}_k$ with output given by

$$Y\,[k] = \mathbf{w}_k^H \mathbf{X}\,[k]\,. \tag{14}$$

Collecting the output of all narrowband beamformers, we have

$$\mathbf{Y} = [\ Y\,[0] \quad Y\,[1] \quad Y\,[2] \quad \ldots \quad Y\,[N-1]\ ]\,. \tag{15}$$

Finally, performing IDFT of $\mathbf{Y}$ yields the output of the DFT beamformer as follows:

$$\mathbf{y} = [\ y\,[0] \quad y\,[1] \quad y\,[2] \quad \ldots \quad y\,[N-1]\ ]\,, \tag{16}$$

where IDFT is defined as

$$y\,[n] = \frac{1}{N} \sum_{k=0}^{N-1} Y\,[k]\, e^{j2\pi nk/N}, \quad n = 0, 1, \ldots, N-1. \tag{17}$$

As we can see from the procedure described above, the block processing mode collects a block of received data containing N snapshots first. After processing the block, it produces N-point outputs simultaneously. In contrast, the sliding window mode processes the data block once a new snapshot is received. The time-domain data block in (9) is updated by pushing in the new snapshot and pulling out the oldest snapshot, and then the procedure of (10)–(15) is carried out. Since it processes the data for each sample time n, the sliding window mode only produces one output at $n = 0$ in each processing as follows [30]:

$$y\,[0] = \frac{1}{N} \sum_{k=0}^{N-1} Y\,[k]. \tag{18}$$

An example of $N = 3$ for DFT beamformers is depicted in Figure 3. The advantage of the sliding window mode is that the IDFT in Figure 2 can be replaced by a simple adder. However, it has to perform DFT more frequently (specifically, about N times) as compared with block processing.

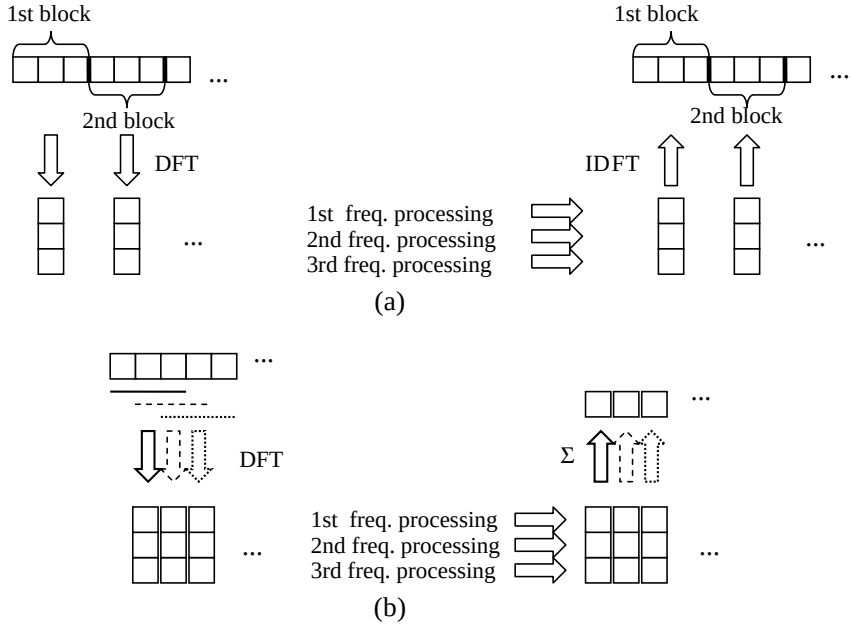

Figure 3. (a) An example of $N = 3$ for the DFT beamformer in block processing mode. (b) An example of $N = 3$ for the DFT beamformer in sliding window mode.

2.3. Generation of Weight Vectors

The MVDR criterion is a typical method to determine the weight vector in narrowband beamforming. By minimizing the total output power and constraining unit-gain in the look direction, the weight vector of the MVDR beamformer in (14) is given by [30]

$$\mathbf{w}_k = \frac{\mathbf{R}_k^{-1}\mathbf{a}_{1,k}}{\mathbf{a}_{1,k}^H\mathbf{R}_k^{-1}\mathbf{a}_{1,k}}, \tag{19}$$

where $(\cdot)^{-1}$ represents matrix inverse,

$$\mathbf{R}_k = E\left[\mathbf{X}\left[k\right]\mathbf{X}^H\left[k\right]\right] \tag{20}$$

is the correlation matrix of the kth frequency bin, and

$$\begin{aligned}\mathbf{a}_{1,k} = [&\exp\left\{j2\pi\left(f_c + f_k\right)\tau_{1,1}\right\} \quad \exp\left\{j2\pi\left(f_c + f_k\right)\tau_{1,2}\right\} \\ &\ldots \quad \exp\left\{j2\pi\left(f_c + f_k\right)\tau_{1,M}\right\}\ ]^T\end{aligned} \tag{21}$$

is the corresponding steering vector. However, the true correlation matrix $\mathbf{R}_k$ is usually unknown and has to be estimated by K snapshots

as follows [23]:

$$\hat{\mathbf{R}}_k = \frac{1}{K}\sum_{i=1}^{K} \mathbf{X}_{(i)}[k]\,\mathbf{X}_{(i)}^H[k], \tag{22}$$

where the subscript (i), $i = 1, 2, \ldots, K$, denotes the ith snapshot of a particular frequency component. Accordingly, the weight vector of (19) becomes

$$\hat{\mathbf{w}}_k = \frac{\hat{\mathbf{R}}_k^{-1}\mathbf{a}_{1,k}}{\mathbf{a}_{1,k}^H\hat{\mathbf{R}}_k^{-1}\mathbf{a}_{1,k}} \tag{23}$$

under finite samples. When the sample size K is large enough, the $\hat{\mathbf{R}}_k$ and $\hat{\mathbf{w}}_k$ may provide good approximations to $\mathbf{R}_k$ and $\mathbf{w}_k$. However, a small K could give a poor estimation and degrade the beamforming performance, which is referred to as the finite sample effect on array processing.

To estimate $\mathbf{R}_k$ using (22), the total data matrix in block processing mode should include K blocks (the $\mathbf{x}$ in (9) denotes one block) as follows:

$$\begin{aligned}\mathbf{x}_B &= \begin{bmatrix}\mathbf{x}_{(1)} & \mathbf{x}_{(2)} & \ldots & \mathbf{x}_{(K)}\end{bmatrix} \\ &= \begin{bmatrix} x_1[0] & x_1[1] & \ldots & x_1[N-1] & x_1[N] \\ x_2[0] & x_2[1] & \ldots & x_2[N-1] & x_2[N] \\ \vdots & \vdots & \ldots & \vdots & \vdots \\ x_M[0] & x_M[1] & \ldots & x_M[N-1] & x_M[N] \end{bmatrix} \\ &\quad \begin{bmatrix} \ldots & x_1[2N-1] & \ldots & x_1[KN-1] \\ \ldots & x_2[2N-1] & \ldots & x_2[KN-1] \\ \ldots & \vdots & \ldots & \vdots \\ \ldots & x_M[2N-1] & \ldots & x_M[KN-1] \end{bmatrix}\end{aligned} \tag{24}$$

since each block contributes only one snapshot $\mathbf{X}_{(i)}[k]$ in (22). On the other hand, the total data matrix producing K snapshots in sliding window mode is given by

$$\mathbf{x}_S = \begin{bmatrix} x_1[0] & x_1[1] & \ldots & x_1[N-1] & x_1[N] & \ldots & x_1[K+N-2] \\ x_2[0] & x_2[1] & \ldots & x_2[N-1] & x_2[N] & \ldots & x_2[K+N-2] \\ \vdots & \vdots & \ldots & \vdots & \vdots & \ldots & \vdots \\ x_M[0] & x_M[1] & \ldots & x_M[N-1] & x_M[N] & \ldots & x_M[K+N-2] \end{bmatrix}$$
$$\text{- -}\mathbf{x}_{(1)}$$
$$\text{- -}\mathbf{x}_{(2)}\ldots. \tag{25}$$

It can be shown that the size of $\mathbf{x}_S$ is smaller than $\mathbf{x}_B$ when $N > 1$ and $K > 1$. However, each block in sliding window mode is highly

correlated and may lead to a worse estimation of $\mathbf{R}_k$. Different from the narrowband case, the total number of snapshots for DFT beamformers depends on the number of frequency bins and the number of snapshots used to estimate $\mathbf{R}_k$ in each frequency bin. If both $N$and K are large, the required memory storage and computational complexity could be amazing. To give a fair comparison to different techniques, the total number of time-domain samples used to estimate $\mathbf{R}_k$ is fixed to J with J being a multiple of N. Thus, $\mathbf{x}_B$ and $\mathbf{x}_S$ with J columns can provide $K_B = J/N$ and $K_S = J - N + 1$ snapshots for each frequency, respectively. Again, it can be shown that $K_B < K_S$ if $N > 1$. As compared with block processing, the sliding window mode gets more frequency-domain snapshots, but at the price of higher correlation for the adjacent snapshots. This difference will be further observed by simulation results.

For the special case of $N = 1$, Equations (10), (20), (19), and (16) are simplified to

$$\mathbf{X} = \mathbf{x} = \mathbf{x}\,[0]\,, \tag{26}$$

$$\mathbf{R} = E\left[\mathbf{X}\,[0]\,\mathbf{X}^H\,[0]\right] = E\left[\mathbf{x}\,[0]\,\mathbf{x}^H\,[0]\right], \tag{27}$$

$$\mathbf{w} = \frac{\mathbf{R}^{-1}\mathbf{a}_{1,0}}{\mathbf{a}_{1,0}^H\mathbf{R}^{-1}\mathbf{a}_{1,0}}, \tag{28}$$

$$\text{and} \quad \mathbf{y} = y\,[0] = \mathbf{w}^H\mathbf{x}\,[0]\,, \tag{29}$$

respectively, when the true correlation matrix $\mathbf{R}$ is known. Note that the results of (26)–(29) are the same for general n because the process $\mathbf{x}(t)$ is stationary. Similarly, we have

$$\mathbf{X}_{(i)} = \mathbf{x}_{(i)} = \mathbf{x}\,[i-1]\,, \tag{30}$$

$$\hat{\mathbf{R}} = \frac{1}{K}\sum_{i=1}^{K}\mathbf{x}\,[i-1]\,\mathbf{x}\,[i-1]^H, \tag{31}$$

$$\hat{\mathbf{w}} = \frac{\hat{\mathbf{R}}^{-1}\mathbf{a}_{1,0}}{\mathbf{a}_{1,0}^H\hat{\mathbf{R}}^{-1}\mathbf{a}_{1,0}}, \tag{32}$$

$$\text{and} \quad \mathbf{y} = y\,[0] = \hat{\mathbf{w}}^H\mathbf{x}\,[0] \tag{33}$$

under finite samples. Therefore, the DFT beamformer with $N = 1$ reduces to the narrowband MVDR beamformer processing the frequency bin f_c only. Moreover, the block processing and sliding window modes are the same in this case whether finite sample effect exists or not.

3. THE OUTPUT SINR OF DFT BEAMFORMERS

It has been shown in Section 2 that the narrowband MVDR beamformer is a special case of the DFT beamformer. Here, we derive the output SINR of DFT beamformers in terms of weight vectors. It is expected that the SINR definition used in narrowband scenario becomes the special case of $N = 1$ and $B \ll f_c$ in our definition.

3.1. The DFT Beamformer with Block Processing

Given a set of weight vectors $\mathbf{w}_k$, $k = 1, 2, \ldots, N$, the array output at the time instant n can be obtained by substituting (14) into (17) as follows:

$$y\,[n]=\frac{1}{N}\sum_{k=0}^{N-1}\mathbf{w}_k^H\mathbf{X}[k]\,e^{j2\pi nk/N}=\frac{1}{N}\mathbf{w}^H\mathbf{F}_n\mathbf{X}_{|},\quad n=0,1,\ldots,N-1, \tag{34}$$

where $\mathbf{w}$ and $\mathbf{X}_{|}$ are column vectors defined by

$$\mathbf{w}\equiv\begin{bmatrix}\mathbf{w}_0^T & \mathbf{w}_1^T & \ldots & \mathbf{w}_{N-1}^T\end{bmatrix}^T, \tag{35}$$

$$\mathbf{X}_{|}\equiv\begin{bmatrix}\mathbf{X}^T[0] & \mathbf{X}^T[1] & \ldots & \mathbf{X}^T[N-1]\end{bmatrix}^T. \tag{36}$$

The $MN \times MN$ matrix $\mathbf{F}_n$ represents the IDFT operation and is related to (12) by

$$\mathbf{F}_n\equiv\begin{bmatrix}\mathbf{I} & 0 & \ldots & 0\\ 0 & e^{j2\pi n/N}\mathbf{I} & & \vdots\\ \vdots & & \ddots & 0\\ 0 & \ldots & 0 & e^{j2\pi n(N-1)/N}\mathbf{I}\end{bmatrix}=\mathrm{diag}\,(\mathbf{e}_n)\otimes\mathbf{I}, \tag{37}$$

where $\mathrm{diag}(\mathbf{e}_n)$ denotes the diagonal square matrix with diagonal entries $\mathbf{e}_n$, $\otimes$ denotes the Kronecker product, and $\mathbf{I}$ is the identity matrix with size $M \times M$. Using (34), the output power of the array is given by

$$E\left\{|y\,[n]|^2\right\}=\frac{1}{N^2}\mathbf{w}^H\mathbf{F}_n\mathbf{R}_{|}\mathbf{F}_n^H\mathbf{w} \tag{38}$$

with

$$\begin{aligned}\mathbf{R}_{|}&\equiv E\left[\mathbf{X}_{|}\mathbf{X}_{|}^H\right]\\ &=\begin{bmatrix}E\left[\mathbf{X}\,[0]\,\mathbf{X}^H\,[0]\right] & E\left[\mathbf{X}\,[0]\,\mathbf{X}^H\,[1]\right] & \ldots & E\left[\mathbf{X}\,[0]\,\mathbf{X}^H\,[N-1]\right]\\ E\left[\mathbf{X}\,[1]\,\mathbf{X}^H\,[0]\right] & E\left[\mathbf{X}\,[1]\,\mathbf{X}^H\,[1]\right] & \ldots & E\left[\mathbf{X}\,[1]\,\mathbf{X}^H\,[N-1]\right]\\ \vdots & \vdots & & \vdots\\ E\left[\mathbf{X}[N-1]\mathbf{X}^H[0]\right] & E\left[\mathbf{X}\,[N-1]\,\mathbf{X}^H[1]\right] & \ldots & E\left[\mathbf{X}[N-1]\mathbf{X}^H[N-1]\right]\end{bmatrix}\end{aligned} \tag{39}$$

denoting the correlation matrix of $\mathbf{X}_{|}$. The correlation matrix $\mathbf{R}_{|}$ is composed of N^2 sub-matrices. Each of the $M \times M$ sub-matrix characterizes the correlation of two frequencies and has the following expression:

$$E\left[\mathbf{X}\left[k_1\right]\mathbf{X}^H\left[k_2\right]\right] = \begin{bmatrix} E\left[X_1\left[k_1\right]X_1^*\left[k_2\right]\right] & E\left[X_1\left[k_1\right]X_2^*\left[k_2\right]\right] & \dots & E\left[X_1\left[k_1\right]X_M^*\left[k_2\right]\right] \\ E\left[X_2\left[k_1\right]X_1^*\left[k_2\right]\right] & E\left[X_2\left[k_1\right]X_2^*\left[k_2\right]\right] & \dots & E\left[X_2\left[k_1\right]X_M^*\left[k_2\right]\right] \\ \vdots & \vdots & \dots & \vdots \\ E\left[X_M\left[k_1\right]X_1^*\left[k_2\right]\right] & E\left[X_M\left[k_1\right]X_2^*\left[k_2\right]\right] & \dots & E\left[X_M\left[k_1\right]X_M^*\left[k_2\right]\right] \end{bmatrix}, \quad (40)$$

where $(\cdot)^*$ denotes the complex conjugate. Using (11), the (m_1, m_2)th entry of $E[\mathbf{X}[k_1]\mathbf{X}^H[k_2]]$ can be further written as

$$E\left[X_{m_1}\left[k_1\right]X_{m_2}^*\left[k_2\right]\right] = \mathbf{e}_{k_1}^H E\left[\tilde{\mathbf{x}}_{m_1}\tilde{\mathbf{x}}_{m_2}^H\right]\mathbf{e}_{k_2} = \mathbf{e}_{k_1}^H \mathbf{R}_{m_1 m_2}\mathbf{e}_{k_2}, \quad (41)$$

where $\mathbf{R}_{m_1 m_2}$ represents the correlation matrix of the time-domain signals received by the m_1th and m_2th array elements. Substituting (41) into (40), we have the explicit expression for the (k_1, k_2)th sub-matrix of $\mathbf{R}_{|}$ given by

$$\begin{aligned} E\left[\mathbf{X}\left[k_1\right]\mathbf{X}^H\left[k_2\right]\right] &= \begin{bmatrix} \mathbf{e}_{k_1}^H\mathbf{R}_{11}\mathbf{e}_{k_2} & \mathbf{e}_{k_1}^H\mathbf{R}_{12}\mathbf{e}_{k_2} & \dots & \mathbf{e}_{k_1}^H\mathbf{R}_{1M}\mathbf{e}_{k_2} \\ \mathbf{e}_{k_1}^H\mathbf{R}_{21}\mathbf{e}_{k_2} & \mathbf{e}_{k_1}^H\mathbf{R}_{22}\mathbf{e}_{k_2} & \dots & \mathbf{e}_{k_1}^H\mathbf{R}_{2M}\mathbf{e}_{k_2} \\ \vdots & \vdots & & \vdots \\ \mathbf{e}_{k_1}^H\mathbf{R}_{M1}\mathbf{e}_{k_2} & \mathbf{e}_{k_1}^H\mathbf{R}_{M2}\mathbf{e}_{k_2} & \dots & \mathbf{e}_{k_1}^H\mathbf{R}_{MM}\mathbf{e}_{k_2} \end{bmatrix} \\ &= \mathbf{E}_{k_1}^H\bar{\mathbf{R}}\mathbf{E}_{k_2}, \end{aligned} \quad (42)$$

where $\mathbf{E}_k$ and $\bar{\mathbf{R}}$ are defined as

$$\mathbf{E}_k \equiv \begin{bmatrix} \mathbf{e}_k & \mathbf{0} & \dots & \mathbf{0} \\ \mathbf{0} & \mathbf{e}_k & \dots & \mathbf{0} \\ \vdots & \vdots & \ddots & \vdots \\ \mathbf{0} & \mathbf{0} & \dots & \mathbf{e}_k \end{bmatrix}_{MN\times M} \quad (43)$$

$$\text{and} \quad \bar{\mathbf{R}} \equiv \begin{bmatrix} \mathbf{R}_{11} & \mathbf{R}_{12} & \dots & \mathbf{R}_{1M} \\ \mathbf{R}_{21} & \mathbf{R}_{22} & \dots & \mathbf{R}_{2M} \\ \vdots & \vdots & & \vdots \\ \mathbf{R}_{M1} & \mathbf{R}_{M2} & \dots & \mathbf{R}_{MM} \end{bmatrix}. \quad (44)$$

Moreover, using the expression of (42), the $\mathbf{R}_{|}$ in (39) can be rewritten as

$$\mathbf{R}_{|} \equiv \begin{bmatrix} \mathbf{E}_0^H\bar{\mathbf{R}}\mathbf{E}_0 & \mathbf{E}_0^H\bar{\mathbf{R}}\mathbf{E}_1 & \dots & \mathbf{E}_0^H\bar{\mathbf{R}}\mathbf{E}_{N-1} \\ \mathbf{E}_1^H\bar{\mathbf{R}}\mathbf{E}_0 & \mathbf{E}_1^H\bar{\mathbf{R}}\mathbf{E}_1 & \dots & \mathbf{E}_1^H\bar{\mathbf{R}}\mathbf{E}_{N-1} \\ \vdots & \vdots & & \vdots \\ \mathbf{E}_{N-1}^H\bar{\mathbf{R}}\mathbf{E}_0 & \mathbf{E}_{N-1}^H\bar{\mathbf{R}}\mathbf{E}_1 & \dots & \mathbf{E}_{N-1}^H\bar{\mathbf{R}}\mathbf{E}_{N-1} \end{bmatrix} = \mathbf{E}^H\bar{\mathbf{R}}\mathbf{E} \quad (45)$$

with

$$\mathbf{E} \equiv [\mathbf{E}_0 \quad \mathbf{E}_1 \quad \ldots \quad \mathbf{E}_{N-1}] \tag{46}$$

denoting the DFT operation. Thus, the array output power at the time instant n in (38) becomes

$$E\left\{|y[n]|^2\right\} = \frac{1}{N^2}\mathbf{w}^H\mathbf{F}_n\mathbf{E}^H\bar{\mathbf{R}}\mathbf{E}\mathbf{F}_n^H\mathbf{w}. \tag{47}$$

Since the D signal sources and noise are mutually uncorrelated, the (m_1, m_2)th sub-matrix of $\bar{\mathbf{R}}$ can be decomposed by using (7) and (9) as follows:

$$\begin{aligned}
\mathbf{R}_{m_1m_2} &= E\left\{\tilde{\mathbf{x}}_{m_1}\tilde{\mathbf{x}}_{m_2}^H\right\} \\
&= \exp\left\{j2\pi f_c\left(\tau_{1,m_1} - \tau_{1,m_2}\right)\right\} \\
&\quad \times \begin{bmatrix} r_1\left(\tau_{1,m_1} - \tau_{1,m_2}\right) & r_1\left(-T_s + \tau_{1,m_1} - \tau_{1,m_2}\right) \\ r_1\left(T_s + \tau_{1,m_1} - \tau_{1,m_2}\right) & r_1\left(\tau_{1,m_1} - \tau_{1,m_2}\right) \\ \vdots & \vdots \\ r_1\left((N-1)T_s + \tau_{1,m_1} - \tau_{1,m_2}\right) & r_1\left((N-2)T_s + \tau_{1,m_1} - \tau_{1,m_2}\right) \end{bmatrix} \\
&\qquad \begin{bmatrix} \ldots & r_1\left(-(N-1)T_s + \tau_{1,m_1} - \tau_{1,m_2}\right) \\ \ldots & r_1\left(-(N-2)T_s + \tau_{1,m_1} - \tau_{1,m_2}\right) \\ & \vdots \\ \ldots & r_1\left(\tau_{1,m_1} - \tau_{1,m_2}\right) \end{bmatrix} \\
&\quad + \ldots + \exp\left\{j2\pi f_c\left(\tau_{D,m_1} - \tau_{D,m_2}\right)\right\} \\
&\quad \times \begin{bmatrix} r_D\left(\tau_{D,m_1} - \tau_{D,m_2}\right) & r_D\left(-T_s + \tau_{D,m_1} - \tau_{D,m_2}\right) \\ r_D\left(T_s + \tau_{D,m_1} - \tau_{D,m_2}\right) & r_D\left(\tau_{D,m_1} - \tau_{D,m_2}\right) \\ \vdots & \vdots \\ r_D((N-1)T_s + \tau_{D,m_1} - \tau_{D,m_2}) & r_D((N-2)T_s + \tau_{D,m_1} - \tau_{D,m_2}) \end{bmatrix} \\
&\qquad \begin{bmatrix} \ldots & r_D\left(-(N-1)T_s + \tau_{D,m_1} - \tau_{D,m_2}\right) \\ \ldots & r_D\left(-(N-2)T_s + \tau_{D,m_1} - \tau_{D,m_2}\right) \\ & \vdots \\ \ldots & r_D\left(\tau_{D,m_1} - \tau_{D,m_2}\right) \end{bmatrix} \\
&\quad + \begin{bmatrix} r_w(0) & 0 & \ldots & 0 \\ 0 & r_w(0) & \ldots & 0 \\ \vdots & \vdots & & \vdots \\ 0 & 0 & \ldots & r_w(0) \end{bmatrix} \delta_{m_1m_2} \\
&\equiv \mathbf{R}_{m_1m_2,s_1} + \ldots + \mathbf{R}_{m_1m_2,s_D} + \mathbf{R}_{m_1m_2,w},
\end{aligned} \tag{48}$$

where $\delta_{m_1m_2}$ denotes the Kronecker delta. Accordingly, the correlation matrix $\bar{\mathbf{R}}$ in (44) and the output power in (47) can be written as follows:

$$\bar{\mathbf{R}} = \bar{\mathbf{R}}_{s_1} + \bar{\mathbf{R}}_{s_2} + \ldots + \bar{\mathbf{R}}_{s_D} + \bar{\mathbf{R}}_w, \tag{49}$$

$$E\left\{|y[n]|^2\right\} = P_{s_1}[n] + P_{s_2}[n] + \ldots + P_{s_D}[n] + P_w[n], \tag{50}$$

where

$$P_{s_d}[n] = \frac{1}{N^2}\mathbf{w}^H\mathbf{F}_n\mathbf{E}^H\bar{\mathbf{R}}_{s_d}\mathbf{E}\mathbf{F}_n^H\mathbf{w}, \quad d = 1, 2, \ldots, D, \tag{51}$$

are the output powers of the signal sources and

$$P_w[n] = \frac{1}{N^2}\mathbf{w}^H\mathbf{F}_n\mathbf{E}^H\bar{\mathbf{R}}_w\mathbf{E}\mathbf{F}_n^H\mathbf{w} = \frac{r_w(0)}{N^2}\left\|\mathbf{E}\mathbf{F}_n^H\mathbf{w}\right\|^2 \tag{52}$$

is the output power of noise. The $||\cdot||$ in (52) denotes Euclidean norm of a vector. Finally, the output SINR of the DFT beamformer with block processing at the time instant n can be defined as

$$SINR[n] = \frac{P_{s_1}[n]}{P_{s_2}[n] + \ldots + P_{s_D}[n] + P_w[n]}. \tag{53}$$

As we will see from the simulation results in Section 5, the output SINRs of the block processing mode at distinct n's could be very different. Because the random processes $s_d(t)$, $d = 1, 2, \ldots, D$, and $w_m(t)$, $m = 1, 2, \ldots, M$, are assumed stationary, the second order statistical properties of $y[n]$ and $y[n + kN]$ are the same for a given weight vector $\mathbf{w}$. Therefore, the output SINR of the DFT beamformer with block processing is periodic with period N.

In summary, the procedure to compute the output SINR of the DFT beamformer with block processing given a set of weight vectors is described as follows:

Step 1: Construct $\mathbf{E}$ using (46), (43), and the definition of $\mathbf{e}_k$ in (12).

Step 2: Construct $\mathbf{F}_n$ from (37) for the time instant n.

Step 3: Compute the output powers of signals and noise from (51) and (52).

Step 4: Compute the array output SINR at the time instant n according to (53).

Step 5: Set $n = n + 1$ and go to step 2. If $n \geq N$, $SINR[n] = SINR[n - N]$.

3.2. The DFT Beamformer with Sliding Window

In the sliding window mode, there is only one output $y[0]$ given by (18) for each cycle. Since $\mathbf{F}_n$ reduces to an identity matrix for $n = 0$, the output power of the sliding window mode becomes

$$E\left\{|y[0]|^2\right\} = \frac{1}{N^2}\mathbf{w}^H\mathbf{E}^H\bar{\mathbf{R}}\mathbf{E}\mathbf{w}. \tag{54}$$

Following the similar derivation in Section 3.1, we get

$$SINR\,[0] = \frac{P_{s_1}\,[0]}{P_{s_2}\,[0] + \ldots + P_{s_D}\,[0] + P_w\,[0]} \tag{55}$$

with

$$P_{s_d}\,[0] \;=\; \frac{1}{N^2}\mathbf{w}^H\mathbf{E}^H\bar{\mathbf{R}}_{s_d}\mathbf{E}\mathbf{w}, \quad d = 1, 2, \ldots, D \tag{56}$$

$$\text{and} \quad P_w\,[0] \;=\; \frac{r_w\,(0)}{N^2}\,\|\mathbf{E}\mathbf{w}\|^2\,. \tag{57}$$

Again, for a given weight vector $\mathbf{w}$, the statistical properties of $y[n]$ are the same for all n's since the signal sources and noise are stationary. Therefore, the results of (54)–(57) are suitable for general n, and the time index [0] can be neglected. The steps for computing the output SINR of the DFT beamformer with sliding window are presented as follows:

Step 1: Construct $\mathbf{E}$ by using (46), (43), and the definition of $\mathbf{e}_k$ in (12).

Step 2: Compute the output powers of signals and noise from (56) and (57).

Step 3: Compute the output SINR according to (55).

Step 4: For $n \neq 0$, $SINR[n] = SINR[0]$.

3.3. The Special Case of $N = 1$ and Narrowband Signal Sources

For the special case of $N = 1$ (narrowband beamformer), both the DFT and IDFT reduce to identity operation, and it is easy to show that

$$\mathbf{E} = \mathbf{E}_0 = \mathbf{F}_0 = \mathbf{I}. \tag{58}$$

In this case, the correlation matrix $\bar{\mathbf{R}}$ can be simplified to

$$\begin{aligned}
\bar{\mathbf{R}} &= E\left[\mathbf{x}\,[0]\,\mathbf{x}^H\,[0]\right] \\
&= \sum_{d=1}^{D}\left[\begin{array}{cc}
r_d\,(0) & r_d\,(\tau_{d,1}-\tau_{d,2})\,e^{j2\pi f_c\left(\tau_{d,1}-\tau_{d,2}\right)} \\
r_d\,(\tau_{d,2}-\tau_{d,1})\,e^{j2\pi f_c\left(\tau_{d,2}-\tau_{d,1}\right)} & r_d\,(0) \\
\vdots & \vdots \\
r_d\,(\tau_{d,M}-\tau_{d,1})\,e^{j2\pi f_c\left(\tau_{d,M}-\tau_{d,1}\right)} & r_d\,(\tau_{d,M}-\tau_{d,2})\,e^{j2\pi f_c\left(\tau_{d,M}-\tau_{d,2}\right)}
\end{array}\right. \\
&\qquad \left.\begin{array}{ccc}
\ldots & r_d\,(\tau_{d,1}-\tau_{d,M})\,e^{j2\pi f_c\left(\tau_{d,1}-\tau_{d,M}\right)} \\
\ldots & r_d\,(\tau_{d,2}-\tau_{d,M})\,e^{j2\pi f_c\left(\tau_{d,2}-\tau_{d,M}\right)} \\
\ddots & \vdots \\
\ldots & r_d\,(0)
\end{array}\right] + \left[\begin{array}{cccc}
r_w\,(0) & 0 & \ldots & 0 \\
0 & r_w\,(0) & \ldots & 0 \\
\vdots & \vdots & \ddots & \vdots \\
0 & 0 & \ldots & r_w\,(0)
\end{array}\right] \\
&\equiv \mathbf{R}_{s_1} + \ldots + \mathbf{R}_{s_D} + \mathbf{R}_w,
\end{aligned} \tag{59}$$

and the SINR expression in (53) or (55) becomes

$$SINR = \frac{\mathbf{w}^H \mathbf{R}_{s_1} \mathbf{w}}{\mathbf{w}^H \mathbf{R}_{s_2} \mathbf{w} + \ldots + \mathbf{w}^H \mathbf{R}_{s_D} \mathbf{w} + \mathbf{w}^H \mathbf{R}_w \mathbf{w}}. \tag{60}$$

Equation (60) is the output SINR of a narrowband beamformer with an arbitrary source bandwidth B. The time index $[n]$ is neglected due to the assumption of stationary sources. Furthermore, if the signals and noise are also narrowband, i.e., $B \ll f_c$, the correlation matrix of (59) can be approximated by

$$\begin{aligned}\bar{\mathbf{R}} &= E\left[\mathbf{x}[0]\,\mathbf{x}^H[0]\right] \\ &\approx \sum_{d=1}^{D} r_d(0) \begin{bmatrix} 1 & e^{j2\pi f_c(\tau_{d,1}-\tau_{d,2})} & \ldots & e^{j2\pi f_c(\tau_{d,1}-\tau_{d,M})} \\ e^{j2\pi f_c(\tau_{d,2}-\tau_{d,1})} & 1 & \ldots & e^{j2\pi f_c(\tau_{d,2}-\tau_{d,M})} \\ \vdots & \vdots & \ddots & \vdots \\ e^{j2\pi f_c(\tau_{d,M}-\tau_{d,1})} & e^{j2\pi f_c(\tau_{d,M}-\tau_{d,2})} & \ldots & 1 \end{bmatrix} \\ &\quad + r_w(0) \begin{bmatrix} 1 & 0 & \ldots & 0 \\ 0 & 1 & \ldots & 0 \\ \vdots & \vdots & \ddots & \vdots \\ 0 & 0 & \ldots & 1 \end{bmatrix} = \sum_{d=1}^{D} r_d(0)\,\mathbf{a}_{d,0}\mathbf{a}_{d,0}^H + r_w(0)\,\mathbf{I}. \end{aligned} \tag{61}$$

It is recognized that the combination of (60) and (61) is exactly the definition of the output SINR commonly used in narrowband beamforming [2, 7], which confirms the validity of the derivation.

3.4. The Special Case of Band-limited White Processes

In broadband research, it is common to assume the signal sources are also band-limited white processes with power levels different from noise. Consider a baseband signal source $z(t)$ with power spectral density (PSD) given by

$$S_z(f) = \begin{cases} P_z, & -B < f < B \\ 0, & \text{else} \end{cases}, \tag{62}$$

where P_z is a parameter controlling the power level of the source. The corresponding autocorrelation function of $z(t)$ is given by [31]

$$r_z(\xi) = E\left[z(t)\,z^*(t-\xi)\right] = 2BP_z \mathrm{sinc}(2B\xi). \tag{63}$$

Under the assumption of white sources, the $\bar{\mathbf{R}}_{s_d}$ in (51) and (56) can be constructed by (63) with $z(t)$ replaced by $s_d(t)$. Because the random processes are sampled at Nyquist rate, i.e., $T_s = 1/2B$, the samples of each element are uncorrelated due to

$$r_z(kT_s) = \begin{cases} 2BP_z, & k = 0 \\ 0, & k \neq 0 \end{cases}. \tag{64}$$

This property is helpful for simulating narrowband signal sources because, as we mentioned in the context of (8), only $s_d(0)$, $s_d(T_s)$, ..., $s_d(JT_s)$ are required. Hence, the sequences can be obtained by generating a series of uncorrelated random variables. However, it becomes more complicated for the broadband sources since $s_d(nT_s + \tau_{d,m})$, $m = 1, 2, \ldots, M$, cannot be approximated by $s_d(nT_s)$. In contrast to the narrowband case, the total points to be produced are $s_d(\tau_{d,1})$, $s_d(\tau_{d,2})$, ..., $s_d(\tau_{d,M})$, $s_d(T_s + \tau_{d,1})$, $s_d(T_s + \tau_{d,2})$, ..., $s_d(T_s + \tau_{d,M})$, ..., $s_d(JT_s + \tau_{d,M})$ (Note that the time is not necessarily in order). The time intervals between these samples are non-uniform. Besides, each pair of them has particular correlation. These problems could make difficulties for simulating broadband signals. On the other hand, no such concern is required to simulate noise in broadband scenario because the noise of each sensor and each sample is uncorrelated (independent, if they are Gaussian).

4. NUMERICAL RESULTS

To evaluate the performance of DFT beamformers, simulations are performed based on the specifications described in the following. An 8-element uniform linear array (ULA) with inter-element spacing equal to half-wavelength at the center frequency is considered. For a ULA with reference point at the first element, the time delay $\tau_{d,m}$ is equal to $(m-1)L\sin\theta_d/C$ with L, θ_d, C denoting the inter-element spacing, direction of arrival off broadside, and propagation velocity, respectively. The baseband signal sources $s_d(t)$ and noise $w_m(t)$ are assumed to be stationary band-limited white circular *Gaussian* processes with autocorrelation function and PSD shown in Figure 4 (the amplitude depends on the strength of the source). The powers and the directions of the signal sources are set to $P_z = 5, 10, 10$ (dB/MHz) above the noise level and $\theta_d = 20°, -20°, 40°$ off array broadside, respectively, where the first one denotes the desired signal and the others interference. The default settings for the center frequency f_c, the signal bandwidth B, the sampling frequency $1/T_s$, the number N of frequency bins, and the total number J of data samples are 150 MHz, 50 MHz, 100 MHz, 10, and 1000, respectively. Moreover, the number of Monte Carlo runs is 10 for showing the output SINRs with finite sample effect.

4.1. Simulation Methodology

The output SINRs are computed by first generating weight vectors with or without finite sample effect and then following the procedures described in Sections 3.1 and 3.2. For the perfect scenario without

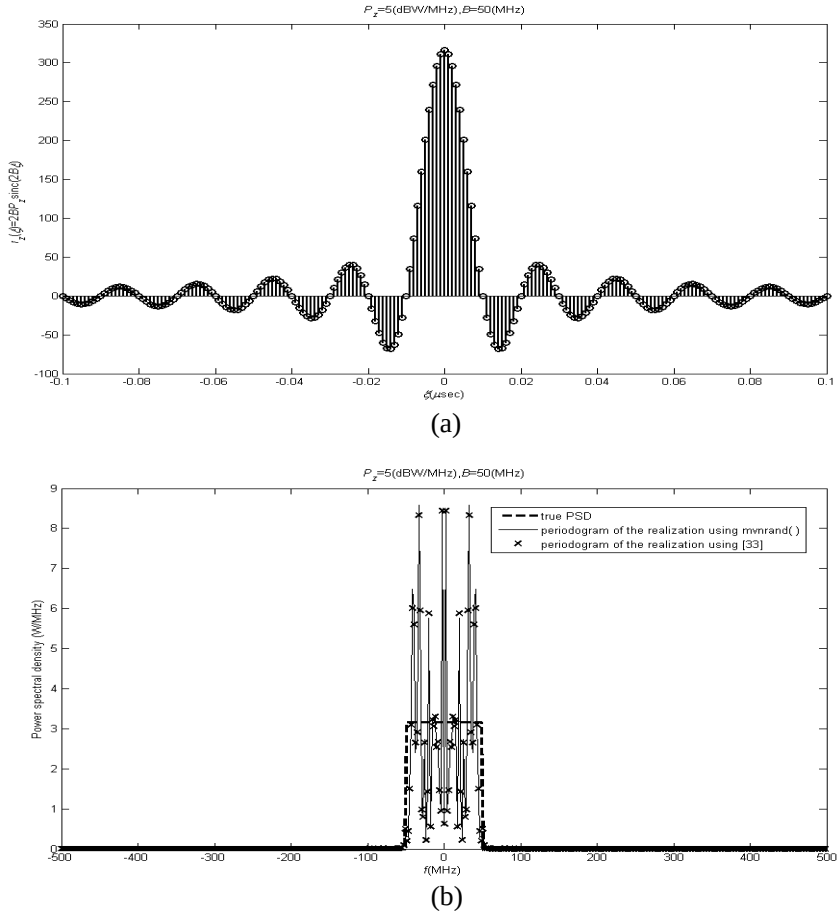

Figure 4. (a) The autocorrelation function of a band-limited white process. (b) The PSD of a band-limited white process.

finite sample effect, the required correlation matrices to produce weight vectors are assumed known and substituted by the explicit expressions derived in (42), (44), and (48). For the case with finite sample effect, a large amount of samples for each band-limited Gaussian source is required to construct the received data matrix $\mathbf{x}_B$ or $\mathbf{x}_S$ and estimate the correlation matrices $\mathbf{R}_k$. In our example, the total number of samples for each random process is $M \times J = 8000$. The samples of each random process are correlated, and the sampling interval is usually non-uniform as discussed in Section 3.4. Traditionally, the realizations of a multivariate Gaussian vector with presumed correlations can be

obtained by transforming the standard normal random variables [32]. However, the vectors and transformation matrix in our case are too huge to be allocated or manipulated for computer simulations. Instead, we adopt the approximation method proposed in [33] to reconstruct the waveform of the random processes and then sample them at adequate time instants. A realization using the *mvnrnd* function of MATLAB and the approximated waveform using the technique in [33] with window size = 10 are compared in Figure 5. The periodograms of the two waveforms are presented in Figure 4(b) as well. The two waveforms and their spectra are very close, which shows the accuracy and validity for the technique in [33]. Another approximation method to generate realizations of a band-limited Gaussian process is reported in [34].

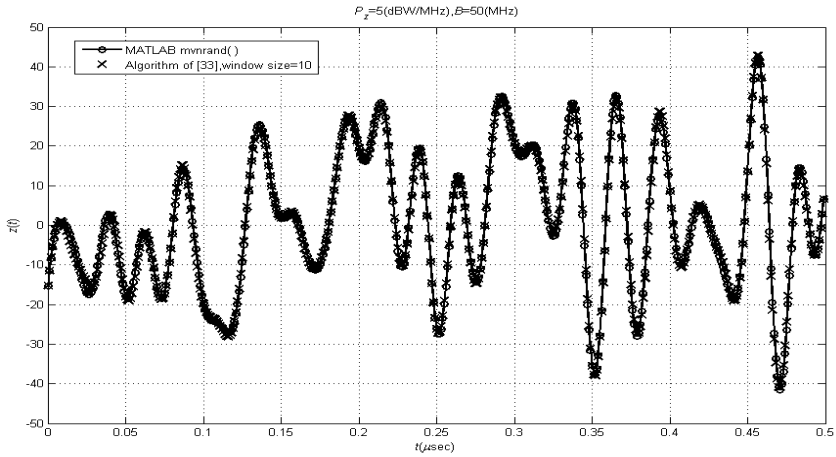

Figure 5. A realization of band-limited white Gaussian process and the approximated waveform using the algorithm of [33].

In addition to the narrowband MVDR and DFT beamformers, we present the results of the popular TDL beamformer [18, 19] for comparison. Since the TDL beamformer assumes the desired signal is incident from array broadside, the presteering time and phase delays are required such that the baseband received signal of (6) becomes

$$x_m(t)\,|_{TDL} = s_1(t) + \sum_{d=2}^{D} s_d(t+\tau_{d,m}-\tau_{1,m}) \exp\{j2\pi f_c(\tau_{d,m}-\tau_{1,m})\} + w_m(t-\tau_{1,m}) \exp\{-j2\pi f_c \tau_{1,m}\}. \quad (65)$$

Similar to the DFT beamformers, the TDL beamformer first storages

a series of received vectors from time instant $n = 0$ to $n = N - 1$ like the way in (9). However, the TDL beamformer weights the time-domain data directly and needs no DFT or IDFT operation. Following the concept of [18], for a particular time instant, the gathered N data vectors are stacked as follows:

$$\mathbf{x}_{TDL} = \left[\begin{array}{cccc} \mathbf{x}^T[N-1] & \mathbf{x}^T[N-2] & \ldots & \mathbf{x}^T[0] \end{array} \right]^T, \tag{66}$$

where $\mathbf{x}[n]$, $n = 0, 1, \ldots, N-1$, are the same as (9) except that the time and phase are presteered in (65). The correlation matrix $\mathbf{R}_{TDL} = E[\mathbf{x}_{TDL}\mathbf{x}_{TDL}^H]$ can be obtained as the similar way in deriving (48), and the well-known linearly constraint minimum variance (LCMV) solution is utilized to obtain the weight coefficients in the TDL beamformer as follows [18, 19]:

$$\begin{aligned} \mathbf{w}_{TDL} &= \mathbf{R}_{TDL}^{-1}\mathbf{C}\left(\mathbf{C}^H\mathbf{R}_{TDL}^{-1}\mathbf{C}\right)^{-1}\mathbf{f}, \\ \mathbf{C} &= \begin{bmatrix} \mathbf{1} & \mathbf{0} & \ldots & \mathbf{0} \\ \mathbf{0} & \mathbf{1} & \ldots & \mathbf{0} \\ \vdots & \vdots & \ddots & \vdots \\ \mathbf{0} & \mathbf{0} & \ldots & \mathbf{1} \end{bmatrix}, \quad \mathbf{f} = \begin{bmatrix} 0 \\ \vdots \\ 0 \\ 1 \end{bmatrix}, \end{aligned} \tag{67}$$

where $\mathbf{1}$ denotes the M-dimensional column vector with all entries equal to 1. The constraint matrix $\mathbf{C}$ and the response vector $\mathbf{f}$ in (67) are assigned to produce unit gain in the look direction. For the situation with finite sample effect, the correlation matrix $\mathbf{R}_{TDL}$ is estimated by averaging $\mathbf{x}_{TDL}\mathbf{x}_{TDL}^H$ obtained from each sampling time instant nT_s. The output SINR of the TDL beamformer is computed by (55)–(57) with $\mathbf{w}$, $\bar{\mathbf{R}}_{s_d}$, and $\mathbf{E}$ replaced by the corresponding TDL weight vector, the TDL correlation matrices, and the identity matrix, respectively. Likewise, the output SINR of the TDL beamformer is time-invariant due to the stationary assumption.

4.2. Demonstration of the Output SINRs

The influences of the number of frequency bins N, the signal bandwidth B, and the number of data samples J on the performance of the DFT beamformers are examined. For notation convenience, the DFT beamformers in block processing and sliding window modes are termed as DFT-BP and DFT-SW, respectively. Besides, we use "known $\mathbf{R}$" and "estimated $\mathbf{R}$" to distinguish the cases without and with finite sample effect. First, we observe the effect of N in Figure 6. Since the performance of DFT-BP is time-variant, we depict its output SINR for $n = 0, 1, \ldots, 39$ without and with finite sample effect in Figures 6(a) and 6(b), respectively. In both figures, the output SINR curves are periodic with period N since the received signal is assumed stationary.

The shape of the curves within $0 \leq n \leq N$ is similar to a hill. It is our experience that the output SINR of DFT-BP usually gets a worse performance at $n = 0$ or $N - 1$ and performs well in the neighborhood of $n = \text{floor}(N/2)$, where $\text{floor}(\cdot)$ represents rounding toward negative infinity. The SINR difference of $n = 0$ and $n = \text{floor}(N/2)$ could be up to several dBs for a particular $N > 1$. This observation implies the weakness of DFT-SW since it always selects the output of DFT-BP at $n = 0$ as its output. For the case without finite sample effect, it is seen

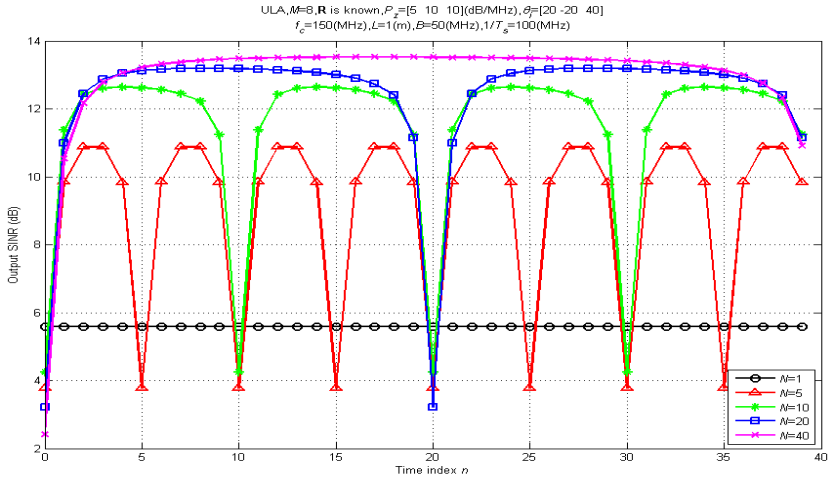

(a)

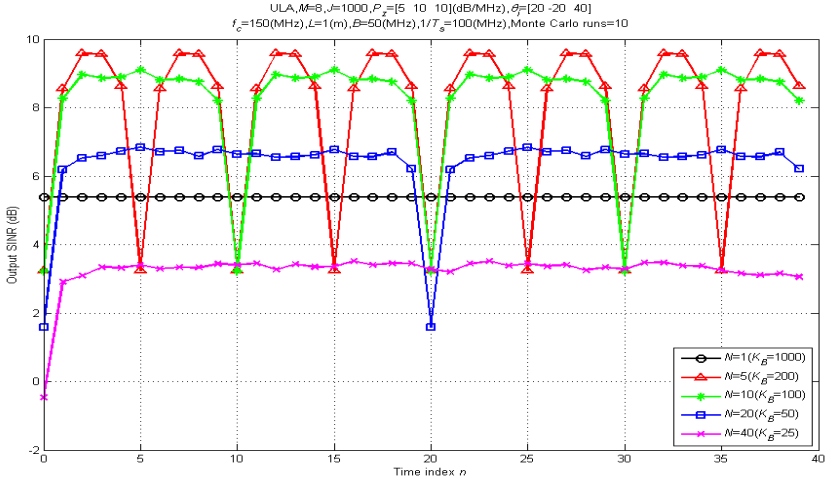

(b)

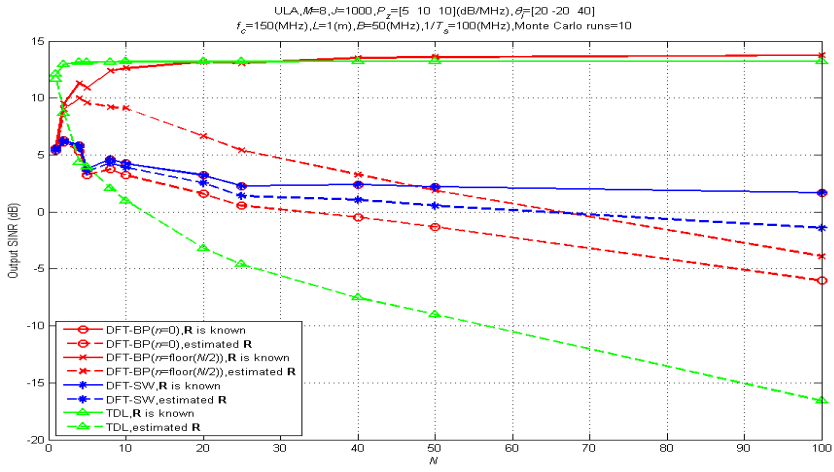

(c)

Figure 6. (a) The output SINRs of DFT-BP with different N. The correlation matrices are assumed known. (b) The output SINRs of DFT-BP with different N. The correlation matrices are estimated by $J = 1000$ samples. (c) The output SINRs of DFT-BP, DFT-SW, and TDL versus N.

from Figure 6(a) that increasing N allows the beamformer processing more frequency bins and improves the output SINR. However, when the total number J of data samples is fixed to 1000, a trade-off between N and K_B can be observed from Figure 6(b). Although the increase of N is conducive to preserve more frequency bins, the performance for each of them is degraded due to the loss of K_B and the poorer estimation of $\mathbf{R}_k$. Selecting $N = 5$, $K_B = 200$ can achieve a higher peak in SINR than the other settings, but its SINR could be lower than narrowband MVDR ($N = 1$, $K_B = 1000$) at $n = 0$. The overall output SINR is degraded when N is increased from 5 to 40. For $N = 40$, $K_B = 25$, the performance of DFT-BP is totally deteriorated by the finite sample effect and is worse than the narrowband MVDR beamformer. The performances of DFT-BP, DFT-SW, and TDL are compared in Figure 6(c). Because the performance difference for DFT-BP at distinct output time could be significant, the SINRs of DFT-BP with $n = 0$ and $n = \text{floor}(N/2)$ are both presented for reference. For the case without finite sample effect, both the output SINRs of TDL and DFT-BP with $n = \text{floor}(N/2)$ are increased with the growth of N. Only 4 or 5 taps are sufficient for TDL to achieve a satisfactory performance, but DFT-BP with $n = \text{floor}(N/2)$ slightly outperforms

TDL for $N \geq 40$. The curves of DFT-BP with $n = 0$ and DFT-SW coincide because their weight vectors with known $\mathbf{R}$ are essentially the same. Their SINRs reach a maximum for $N = 2$ and then degrade gradually for larger N's. For the case with finite sample effect, we can see that the performance of TDL is deteriorated significantly and depressed with the growth of N. This phenomenon can be attributed to the more demand of data samples for TDL because the size of the estimated correlation matrix ($MN \times MN$) is inflated rapidly. The DFT-BP with $n = \text{floor}(N/2)$ outperforms the other methods for most of N's under finite samples. However, its performance is degraded for $N > 10$ due to the worse estimation of correlation matrices. Here, it is noted that the results of DFT-BP with $n = 0$ and DFT-SW are not the same because their correlation matrices are estimated in different ways. The two curves have similar trends, but DFT-SW slightly outperforms DFT-BP with $n = 0$. Based on the observation above, we may conclude that a higher number of frequency bins does not necessarily guarantee a better performance for DFT beamformers. Especially, when the correlation matrices are estimated by finite samples, there exists certain compromise between the number of frequency bins and the number of snapshots for estimating correlation matrices.

Next, we examine the influence of the signal bandwidth B in Figure 7. Figures 7(a) and 7(b) demonstrate the output SINRs of DFT-BP and narrowband MVDR for $n = 0, 1, \ldots, 9$ without and with finite sample effect, respectively. In Figure 7(a), the narrowband MVDR beamformer slightly outperforms DFT-BP for $B = 1\,\text{MHz}$. However, as the signal bandwidth increases, the performance of narrowband MVDR degrades more seriously than DFT-BP. When the signal bandwidth is increased to 100 MHz, the output SINR of narrowband MVDR is below 0dB, which means the desired signal is corrupted by the interference and noise in array output. In contrast, the performance of DFT-BP is more insensitive to the variation of the signal bandwidth B. Similar phenomenon can be seen from Figure 7(b). Comparing Figures 7(a) and 7(b), we see that the curves of narrowband MVDR are almost unchanged because the number of data samples is large ($J = 1000$) for $N = 1$. Although DFT-BP has more decay in overall performance due to finite samples, its steady state of the output SINRs (i.e., $n = 3 \sim 9$) concentrates in 7–10 dB despite of the great variation of B. This exhibits the better capability of DFT-BP in addressing the broadband signals and noise. The output SINRs of narrowband MVDR, DFT-BP with $n = 0$, DFT-BP with $n = 5$, DFT-SW, and TDL versus B are compared in Figure 7(c). When the true correlation matrix $\mathbf{R}$ is used, the performances of TDL and DFT-BP with $n = 5$ are almost invariant to signal bandwidth, whereas those of DFT-BP

with $n = 0$, DFT-SW, and narrowband MVDR are degraded with the growth of B. TDL has the highest output SINR until $B \geq 90\,\text{MHz}$. DFT-BP with $n = 0$ or DFT-SW outperforms the narrowband MVDR beamformer for $B \geq 70\,\text{MHz}$. However, choosing $n = 5$ for DFT-BP improves the performance greatly and reduces this bandwidth margin from 70 MHz to 20 MHz. When these beamformers suffer finite sample effect, it is noted that TDL has significant degeneration and poorest performance as compared with the other broadband beamformers. In contrast, although DFT-BP with $n = 5$ is degraded about 4 dB in

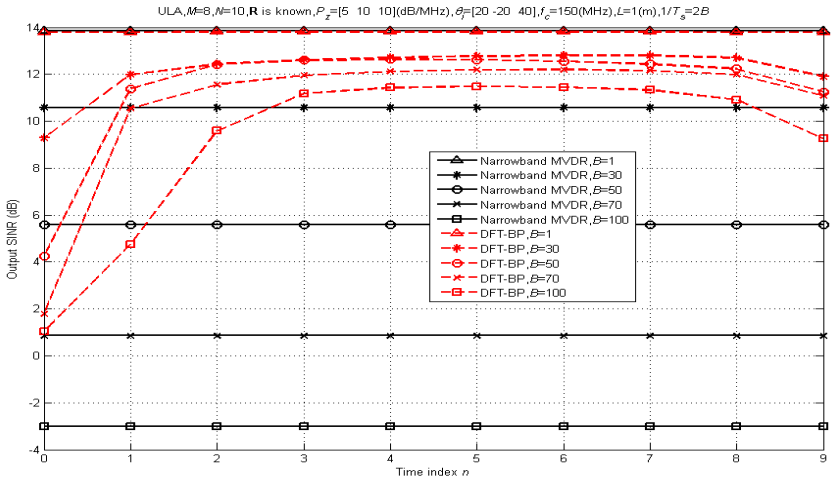

(a)

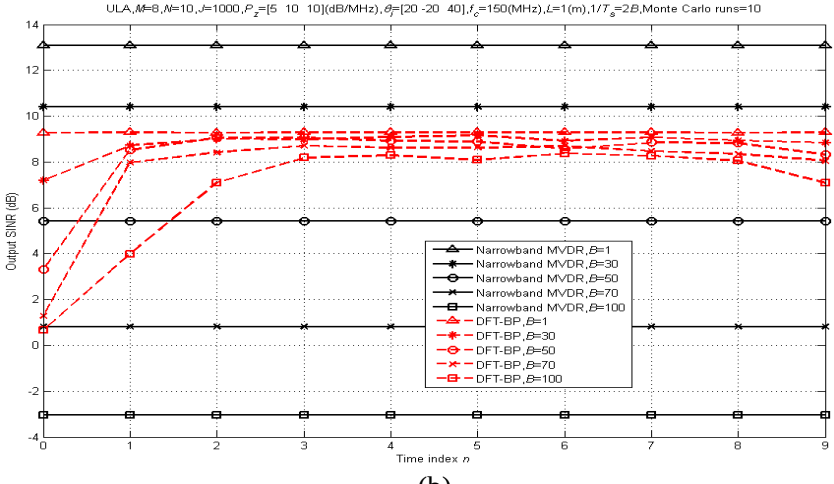

(b)

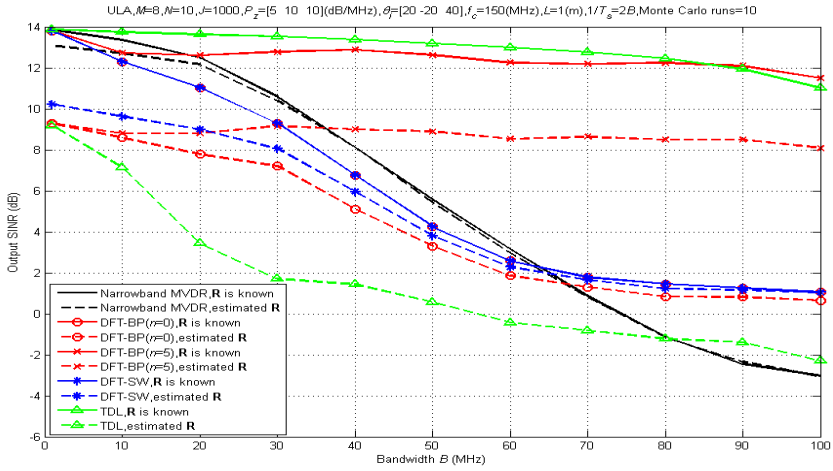

(c)

Figure 7. (a) The output SINRs of DFT-BP with different B. The correlation matrices are assumed known. (b) The output SINRs of DFT-BP with different B. The correlation matrices are estimated by $J = 1000$ samples. (c) The output SINRs of narrowband MVDR, DFT-BP, DFT-SW, and TDL versus B.

output SINR due to finite samples, its performance is superior to the other methods for $B \geq 40\,\text{MHz}$. The curves of DFT-BP with $n = 0$ and DFT-SW have similar trends, but the output SINR of DFT-SW is a little higher. Again, since the number of data samples is sufficient for $N = 1$ in this case, the curves of narrowband MVDR with and without finite sample effect are close. In summary, although TDL performs well in the broadband environment when the correlation matrix is known, its performance can be encumbered by the finite sample effect and poorer than the narrowband MVDR beamformer. The simulation results indicate DFT-BP with $n = 5$ is a better choice for broadband beamforming when the finite sample effect is present.

The influence of J on the beamformers is presented in Figure 8. Figure 8(a) shows the output SINRs of DFT-BP for $n = 0, 1, \ldots, 9$ with and without finite sample effect. We can see that the output SINR lies between -2 and $2\,\text{dB}$ when the number of data samples for estimating $\mathbf{R}_k$ (i.e., K_B) is equal to twice of the number of array elements. The performance of DFT-BP can be enhanced by increasing the sample size K_B. When K_B is increased to 200, the difference between the output SINRs with and without finite sample effect is within $3\,\text{dB}$. As the former investigation [5] for narrowband

beamforming, the required number of data samples to attain 3 dB difference from the optimal SINR is usually larger than twice of the number of elements when the received data vector contains the desired signal. The convergence behavior of the beamformers is compared in Figure 8(b). As we observed before, the narrowband MVDR

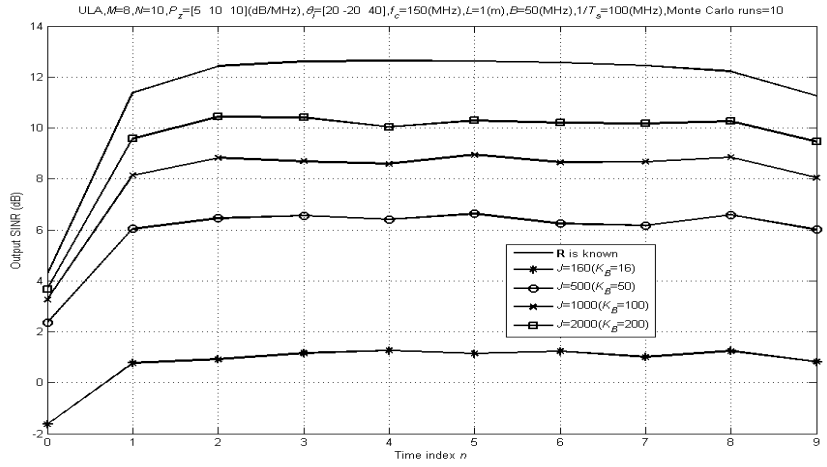

(a)

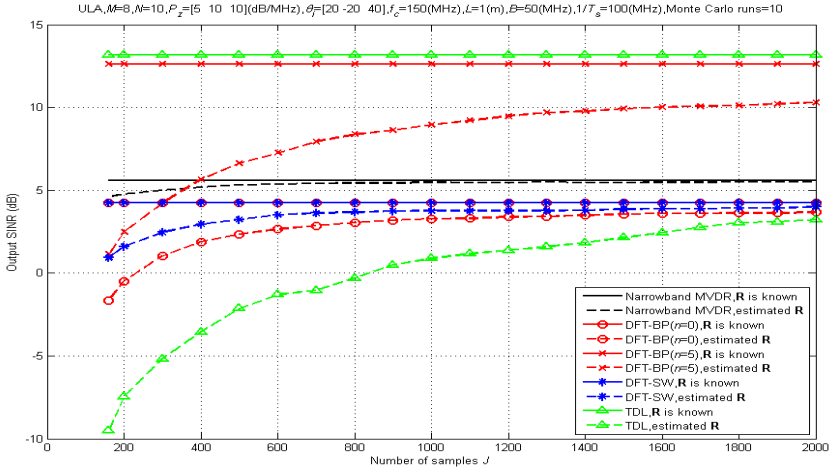

(b)

Figure 8. (a) The output SINRs of DFT-BP with different J. (b) The output SINRs of narrowband MVDR, DFT-BP, DFT-SW, and TDL versus J.

beamformer is less sensitive to the data sample size and converges faster than the other methods. The output SINRs of DFT-BP with $n = 0$ and DFT-SW also reach their steady states quickly but are bounded by the poor optimal performance. Again, DFT-SW slightly outperforms DFT-BP with $n = 0$ under finite samples, which implies the sliding window mode could estimate the correlation matrices more precisely than block processing. Although TDL and DFT-BP with $n = 5$ have satisfactory performance when the true correlation matrices are used, both of them suffer from slow convergence rate under finite samples. The output SINR of DFT-BP with $n = 5$ still transcends those of the other methods for $J \geq 400$, but TDL is greatly affected by the finite sample effect and has the worst performance. This observation reveals the necessity to develop robust methods for alleviating the finite sample effect in broadband beamforming.

5. CONCLUSION

The output SINRs of DFT beamformers using true correlation matrices and finite sample estimations are investigated in this paper. Based on this work, it is shown that the DFT beamformers have better capability to deal with broadband sources than the narrowband MVDR beamformer. As compared with the broadband TDL beamformer, the DFT beamformers are less sensitive to the finite sample effect in broadband environments. However, the number N of frequency bins in DFT beamformers should be carefully assigned especially when the total sample size for estimation is limited. Dividing the frequency band to more bins does not necessarily yield a better performance because of the worse estimation of the correlation matrices. Moreover, the output SINR of the DFT beamformer in block processing mode at distinct time instant n's can be very different. In our experience, it usually performs well in the middle ($n = \text{floor}(N/2)$) and bad in the beginning ($n = 0$) or the end ($n = N - 1$) of the output block. Since the DFT beamformer in sliding window mode always takes the output at $n = 0$, this discovery encourages us to develop a new structure with a better performance than the existing sliding window mode. Besides, the influence of the finite sample effect on broadband beamformers can be significant according to our investigation. Therefore, it is worth developing robust methods for alleviating the finite sample effect in broadband scenario and exploring the application of the current results on periodical unit cells based metamaterial structures for the future research.

ACKNOWLEDGMENT

This work was supported by the National Science Council of TAIWAN under Grant NSC100-2221-E002-200-MY3.

REFERENCES

1. Gu, Y. J., Z.-G. Shi, K. S. Chen, and Y. Li, "Robust adaptive beamforming for a class of Gaussian steering vector mismatch," *Progress In Electromagnetics Research*, Vol. 81, 315–328, 2008.
2. Mestre, X. and M. A. Lagunas, "Finite sample size effect on minimum variance beamformers: optimum diagonal loading factor for large arrays," *IEEE Trans. Signal Process.*, Vol. 54, No. 1, 69–82, Jan. 2006.
3. Li, W.-X., Y.-P. Li, and W.-H. Yu, "On adaptive beamforming for coherent interference suppression via virtual antenna array," *Progress In Electromagnetics Research*, Vol. 125, 165–184, 2012.
4. Lee, J.-H. and Y.-L. Chen, "Performance analysis of antenna array beamformers with mutual coupling effects," *Progress In Electromagnetics Research B*, Vol. 33, 291–315, 2011.
5. Chang, L. and C.-C. Yeh, "Performance of DMI and eigenspace-based beamformers," *IEEE Trans. Antennas Propag.*, Vol. 40, No. 11, 1336–1347, Nov. 1992.
6. Carlson, B. D., "Covariance matrix estimation errors and diagonal loading in adaptive arrays," *IEEE Trans. Aerosp. Electron. Syst.*, Vol. 24, No. 4, 397–401, Jul. 1988.
7. Chen, Y.-L. and J.-H. Lee, "Finite data performance analysis of LCMV antenna array beamformers with and without signal blocking," *Progress In Electromagnetics Research*, Vol. 130, 281–317, 2012.
8. Pillai, S. U., *Array Signal Processing*, Springer-Verlag, New York, 1989.
9. Rennie, L. L., "The TAP III beamforming system," *IEEE J. Ocean. Eng.*, Vol. 6, No. 1, 18–25, Jan. 1981.
10. Guerci, J. R., J. S. Goldstein, and I. S. Reed, "Optimal and adaptive reduced-rank STAP," *IEEE Trans. Aerosp. Electron. Syst.*, Vol. 36, No. 2, 647–663, Apr. 2000.
11. Tuan, D.-H. and P. Russer, "Signal processing for wideband smart antenna array applications," *IEEE Microw. Mag.*, Vol. 5, No. 1, 57–67, Mar. 2004.
12. Spriet, A., M. Moonen, and J. Wouters, "Robustness analysis

of multichannel Wiener filtering and generalized sidelobe cancellation for multimicrophone noise reduction in hearing aid applications," *IEEE Trans. Speech Audio Process.*, Vol. 13, No. 4, 487–503, Jul. 2005.

13. Compton, R. T., *Adaptive Antennas*, Prentice Hall, New Jersey, 1988.
14. Monzingo, R. A. and T. W. Miller, *Introduction to Adaptive Arrays*, John Wiley & Sons, New York, 1980.
15. Van Veen, B. D. and K. M. Buckley, "Beamforming: A versatile approach to spatial filtering," *IEEE ASSP Magazine*, Vol. 5, No. 2, 4–24, Apr. 1988.
16. Liu, W., "Adaptive wideband beamforming with sensor delay-lines," *Signal Processing*, Vol. 89, 876–882, 2009.
17. Lin, M., W. Liu, and R. J. Langley, "Performance analysis of an adaptive broadband beamformer based on a two-element linear array with sensor delay-line processing," *Signal Processing*, Vol. 90, 269–281, 2010.
18. Frost, O. L., "An algorithm for linearly constrained adaptive array processing," *Proc. IEEE*, Vol. 60, No. 8, 926–935, Aug. 1972.
19. Liu, W. and S. Weiss, *Wideband Beamforming: Concepts and Techniques*, Wiley, Chichester, UK, 2010.
20. Wang, B. H., H. T. Hui, and M. S. Leong, "Optimal wideband beamforming for uniform linear arrays based on frequency-domain MISO system identification," *IEEE Trans. Antennas Propag.*, Vol. 58, No. 8, 2580–2587, Aug. 2010.
21. Zhao, Y., W. Liu, and R. J. Langley, "Adaptive wideband beamforming with frequency invariance constraints," *IEEE Trans. Antennas Propag.*, Vol. 59, No. 4, 1175–1184, Apr. 2011.
22. Hossain, M. S., G. N. Milford, M. C. Reed, and L. C. Godara, "Efficient robust broadband antenna array processor in the presence of look direction errors," *IEEE Trans. Antennas Propag.*, Vol. 61, No. 2, 718–727, Feb. 2013.
23. Godara, L. C., "Application of the fast Fourier transform to broadband beamforming," *J. Acoust. Soc. Am.*, Vol. 98, No. 1, 230–240, Jul. 1995.
24. Godara, L. C. and M. R. Sayyah Jahromi, "Limitations and capabilities of frequency domain broadband constrained beamforming schemes," *IEEE Trans. Signal Process.*, Vol. 47, No. 9, 2386–2395, Sep. 1999.
25. Godara, L. C. and M. R. Sayyah Jahromi, "Convolution constraints for broadband antenna arrays," *IEEE Trans.*

Antennas Propag., Vol. 55, No. 11, 3146–3154, Nov. 2007.

26. Kamiya, Y. and Y. Karasawa, "Performance comparison and improvement in adaptive arrays based on time- and frequency-domain signal processing," *Electronics and Communications in Japan (Part III: Fundamental Electronic Science)*, Vol. 85, No. 9, 35–42, 2002.
27. Zhang, Y., K. Yang, M. G. Amin, and Y. Karasawa, "Performance analysis of subband arrays," *IEICE Trans. Commun.*, Vol. E84-B, No. 9, 2507–2515, Sep. 2001.
28. Zhang, Y., K. Yang, and M. G. Amin, "Subband array implementations for space-time adaptive processing," *EURASIP J. Appl. Signal Process.*, Vol. 2005, No. 1, 99–111, 2005.
29. Compton, R. T., "The relationship between tapped delay-line and FFT processing in adaptive arrays," *IEEE Trans. Antennas Propag.*, Vol. 36, No. 1, 15–26, Jan. 1988.
30. Van Trees, H. L., *Optimum Array Processing*, John Wiley & Sons, New York, 2002.
31. Haykin, S., *Communication Systems*, John Wiley & Sons, New Jersey, 2001.
32. Scheuer, E. M. and D. S. Stoller, "On the generation of normal random vectors," *Technometrics*, Vol. 4, No. 2, 278–281, 1962.
33. Grigoriu, M., "Simulation of stationary process via a sampling theorem," *Journal of Sound and Vibration*, Vol. 166, No. 2, 301–313, 1993.
34. Miller, S. L. and D. Childers, *Probability and Random Processes with Applications to Signal Processing and Communications*, Elsevier, Boston, 2004.